Accumulation of heavy particles in *N*-vortex flow on a disk

Rutger H.A. IJzermans[a] and Rob Hagmeijer
*Department of Mechanical Engineering, University of Twente, P.O. Box 217, 7500 AE Enschede,
The Netherlands*

The motion of heavy particles in potential vortex flows on the unit disk is investigated theoretically and numerically. Configurations with one vortex and with two vortices are considered. In both cases, each vortex follows a regular path on the disk. In the one-vortex case, it is shown that small, heavy particles may accumulate in elliptic regions of the flow, counter-rotating with respect to the vortex. When the particle Stokes number exceeds a threshold depending on the vortex configuration, all particles are expelled from the circular domain. A stability criterion for particle accumulation is derived analytically and verified by numerical results. In the two-vortex case, heavy particles are shown to accumulate in elliptic islands of regular motion. Again, this result is explained by a stability analysis. The results may be useful in the design of gas-particle separators containing a helical vortex filament. © *2006 American Institute of Physics*. [DOI: 10.1063/1.2212987]

I. INTRODUCTION

Gas-particle and gas-condensate separators are widely used in industry.[1,2] Their purpose is to separate small dust particles or small liquid droplets from gas flows. In general the separators consist of a cylindrical tube containing a region of high vorticity. In some applications the vorticity is concentrated in a helical vortex filament. The goal of the present research is to determine the influence of such a coherent structure of vorticity on the motion of heavy particles. The configuration of a steady helical vortex filament in a cylindrical tube is sketched in Fig. 1. The instantaneous three-dimensional potential velocity field induced by a helical vortex filament in an unbounded space follows from the Biot-Savart law and was studied in detail by Hardin.[3] The analysis was extended to a helical vortex filament in a cylindrical tube by Alekseenko *et al.*[4] The calculation of this velocity field is far from trivial due to the torsion of the helical vortex filament.

If, however, the pitch of the helix is very large compared to the tube radius R, the contribution due to the three-dimensionality of the helical vortex filament vanishes.[4] In this limit, the velocity field reduces to a superposition of a constant axial velocity U and a time-dependent two-dimensional flow in the cross-sectional plane, moving with U, as sketched in Fig. 1. The two-dimensional flow is characterized by an eccentrically placed point vortex in a circular domain. In the present paper, the case of two point vortices in a circular domain is considered, too. This corresponds to the motion of two entangled vortex filaments, again in the limit of a very slender tube.

The motion of one point vortex on a disk has been considered already by Lamb.[5] The solution makes use of an image vortex placed outside the disk in order to satisfy the boundary condition on the wall. Due to the velocity induced by the image vortex, the vortex describes a steady circular motion. In a frame rotating with the vortex, the flow field is steady and the motion of passive tracers follows from a time-independent stream function. The self-induced motion of two vortices on a disk is more complicated, but is still regular and integrable. A fairly broad classification of possible orbits has been given by Boffetta *et al.*[6] The case of two point vortices on a disk is special, since it can create a flow that displays chaotic advection of passive tracers despite the regularity of the vortex motion. In this sense, the case of two point vortices on a disk is comparable to the situation of three vortices on an infinite plane.[7]

The dynamics of heavy particles in dilute suspensions has received much attention in the past two decades. Various investigations (e.g., Refs. 8 and 9) have reported the behavior of small heavy particles in flows around fixed vortices. The general conclusion is that heavy particles are expelled from regions of high vorticity and tend to accumulate in regions of high strain. If the centrifugal motion from the vortex centers is balanced by another force such as gravity, a group of heavy particles may be attracted to a single trajectory. This was shown to happen in a Burgers vortex[10] and in a plane mixing layer.[11]

The motion of heavy particles in rotating two-dimensional flows has been investigated in the context of planet formation in the solar nebula (e.g., Refs. 12 and 13). The solar nebula is a collection of gas particles situated on a large disk, whose rotation is described by the laws of Kepler. If it is assumed that the turbulent flow in the solar nebula is approximately two-dimensional, large coherent vortex structures are likely to occur. Bracco *et al.*[12] show that heavy particles tend to accumulate in large anticyclonic vortices, i.e., vortices with sign opposite to the major Keplerian rotation. Chavanis[14] derives an analytical estimate of the time it takes to capture a heavy particle in an anticyclonic vortex, by assuming the flow to be a superposition of a prescribed elliptic patch of uniform vorticity and a steadily rotating Keplerian disk; both the particle inertia and the gravitational

[a]Author to who correspondence should be addressed. Telephone: +31 53 4892493. Fax: +31 53 4893695. Electronic mail: r.h.a.ijzermans@ctw.utwente.nl
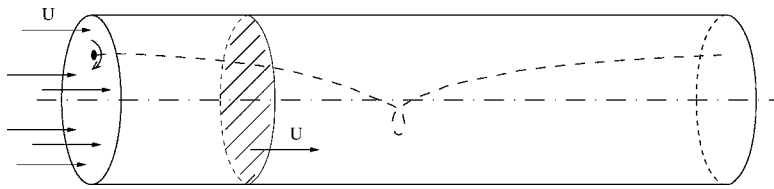
FIG. 1. Helical vortex filament in a gas-liquid separator. In the cross section indicated, the flow may be approximated by a point vortex on a disk.

influence of the star in the center of the disk are taken into account. An overview of the motion of heavy particles in two-dimensional flow is provided by Provenzale,[15] who pays attention to flows generated by a large number of point vortices on an infinite plane and to the case of a finite vorticity distribution on a Keplerian disk.

In the present paper we investigate the motion of heavy particles in a closed circular domain containing one or two point vortices. The presence of the boundary gives rise naturally to a rotation of the flow field.[16] The focus in this paper is on the accumulation of particles due to their inertia in sufficiently dilute flows. In order to isolate the effect of the particle inertia, the simulations are based on a one-way coupling. Gravity is neglected, since it is typically a minor effect in high-speed industrial gas-liquid separators. A stability criterion for particle accumulation is derived and verified numerically for the one-vortex case. Stability is proven for small heavy particles in both the one-vortex and the two-vortex case.

The paper is organized as follows. In Sec. II we present the dynamical equations governing the motion of point vortices on a unit disk, and the equation of motion of passive tracers. In addition, the equations of motion for heavy particles are introduced. In Sec. III we present and discuss the numerical results of motion of heavy particles in a circular domain containing one vortex. The motion of heavy particles in a circular domain containing two vortices is considered in Sec. IV. Finally, a summary and conclusions are given in Sec. V.

II. GOVERNING EQUATIONS

A. Flow field

Consider a closed circular domain with radius R, containing a potential flow generated by N point vortices. In the following, all variables are made dimensionless by choosing R as the characteristic length and the strength of the first vortex Γ_1 as the characteristic circulation. The position of the jth vortex is given by its radial position r_j and angle θ_j, while its strength is Γ_j. For each vortex j, an image vortex with strength $-\Gamma_j$ is placed on the position (r_j^{-1}, θ_j) in order to satisfy the boundary condition of zero normal velocity at $r=1$. Since the velocity field is divergence-free ($\nabla \cdot \boldsymbol{u}=0$), the motion of passive tracers is governed by a stream function which plays the role of a Hamiltonian.

The stream function Ψ is conveniently described in polar coordinates,

$$\Psi(r,\theta) \equiv \sum_{j=1}^{N} \Gamma_j[\Psi_V(r,\theta,r_j,\theta_j) - \Psi_I(r,\theta,r_j,\theta_j)], \quad (1)$$

with

$$\Psi_V(r,\theta,r_j,\theta_j) \equiv -\frac{1}{4\pi}\ln[r^2 + r_j^2 - 2rr_j\cos(\theta-\theta_j)], \quad (2)$$

and

$$\Psi_I(r,\theta,r_j,\theta_j) \equiv \Psi_V(r,\theta,r_j^{-1},\theta_j). \quad (3)$$

The function $\Psi_V(r,\theta,r_j,\theta_j)$ represents the partial stream function corresponding to the jth vortex, whereas $\Psi_I(r,\theta,r_j,\theta_j)$ represents the partial stream function corresponding to the image of the jth vortex. The velocity field is obtained by the canonical equations,

$$u_r = \frac{1}{r}\frac{\partial\Psi}{\partial\theta}, \quad u_\theta = -\frac{\partial\Psi}{\partial r}. \quad (4)$$

The motion of the point vortices itself is governed by Hamiltonian dynamics. The Hamiltonian H is chosen as

$$H = \sum_{i=1}^{N}\sum_{j=i+1}^{N}\Gamma_i\Gamma_j\left[\Psi_V(r_i,\theta_i,r_j,\theta_j) - \Psi_I(r_i,\theta_i,r_j,\theta_j)\right.$$
$$\left. + \frac{1}{4\pi}\ln r_j^2\right] - \frac{1}{2}\sum_{i=1}^{N}\Gamma_i^2\left[\Psi_I(r_i,\theta_i,r_i,\theta_i) - \frac{1}{4\pi}\ln r_i^2\right]. \quad (5)$$

The velocities of the vortices are finally obtained from the canonical equations,

$$\Gamma_i\dot{r}_i = \frac{1}{r_i}\frac{\partial H}{\partial\theta_i}, \quad \Gamma_i r_i\dot{\theta}_i = -\frac{\partial H}{\partial r_i}, \quad (6)$$

where the dots indicate differentiation with respect to time.

During the motion of N point vortices on a disk, two quantities are conserved. The first conserved quantity is the Hamiltonian H defined by Eq. (5). The second conserved quantity is the angular momentum L^2, defined as

$$L^2 \equiv \sum_{i=1}^{N}\Gamma_i r_i^2. \quad (7)$$

Its conservation follows from the rotational symmetry of the disk.[16]

B. Flow field for *N*=1

As an example, we consider a single point vortex with unit strength on the unit disk. The Hamiltonian, given by Eq. (5), reduces to

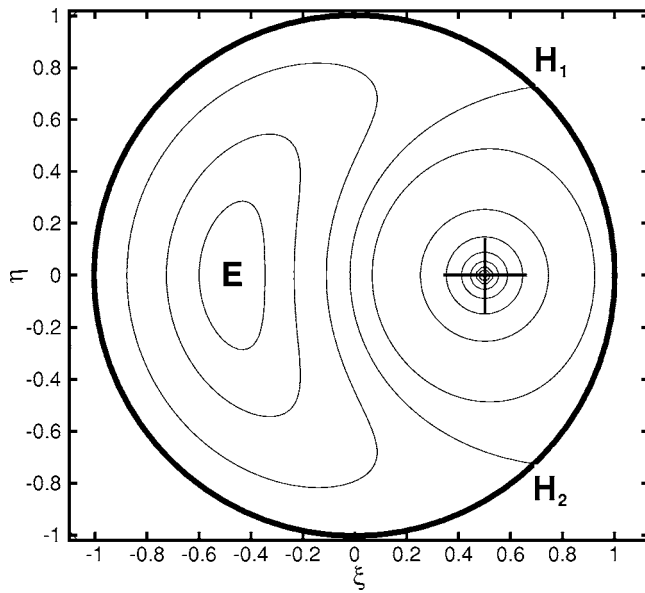$$H = \frac{1}{4\pi}\ln[1-r_1^2]. \quad (8)$$

The motion of the vortex is

FIG. 2. Contour lines of stream function in a one-vortex system, plotted in the frame rotating with vortex 1; $L^2=0.25$. H_1 and H_2 are hyperbolic stagnation points, and E is an elliptic stagnation point.

$$\dot{r}_1 = 0, \quad \dot{\theta}_1 = \frac{1}{2\pi}\frac{1}{1-r_1^2}, \tag{9}$$

which shows that the vortex moves on a circle with constant angular velocity.

When we choose a reference frame that corotates with the vortex, $\phi \equiv \theta - \theta_1$, the stream function becomes

$$\hat{\Psi}(r,\phi) \equiv \Psi(r,\phi+\theta_1) + \tfrac{1}{2}r^2\dot{\theta}_1, \tag{10}$$

with corresponding velocity components

$$u_r = \frac{1}{r}\frac{\partial\hat{\Psi}}{\partial\phi}, \quad u_\phi = -\frac{\partial\hat{\Psi}}{\partial r}. \tag{11}$$

Comparison of the expression for $\hat{\Psi}$ with Ref. 4 shows that it corresponds to the stream function obtained for the flow field induced by a helical vortex filament in a tube, in the limit of infinite pitch.

Contour lines of the stream function are plotted in Fig. 2 for $L^2=0.25$ (see also Ref. 16, p. 135). Three stagnation points in the corotating frame can be distinguished: E is an elliptic stagnation point, and H_1 and H_2 denote two hyperbolic stagnation points. The character of the stagnation points is determined by the Hessian of the stream function evaluated in the stagnation point, $\mathcal{H}_0$,

$$\mathcal{H}_0 < 0 \Leftrightarrow \text{saddle point (hyperbolic point)},$$
$$\mathcal{H}_0 > 0 \Leftrightarrow \text{extremum (elliptic point)}. \tag{12}$$

The Hessian $\mathcal{H}$ is defined as

$$\mathcal{H} \equiv \left(\frac{\partial^2\hat{\Psi}}{\partial\xi^2}\right)\left(\frac{\partial^2\hat{\Psi}}{\partial\eta^2}\right) - \left(\frac{\partial^2\hat{\Psi}}{\partial\xi\,\partial\eta}\right)^2, \quad (r,\theta) \ne (r_1,\theta_1), \tag{13}$$

where $\xi \equiv r\cos\phi$ and $\eta \equiv r\sin\phi$. With Eq. (10) and $\nabla^2\Psi=0$, it follows that

$$\mathcal{H} \equiv -\left(\frac{\partial^2\Psi}{\partial x^2}\right)^2 - \left(\frac{\partial^2\Psi}{\partial x\,\partial y}\right)^2 + \dot{\theta}_1^2, \tag{14}$$

where $x=r\cos\theta$ and $y=r\sin\theta$. Thus, in a fixed frame, $\mathcal{H}<0$ everywhere, so that critical points can only be saddle points.[17] In a rotating frame, however, elliptic stagnation points do exist, provided $\dot{\theta}_1$ is sufficiently large. The rotation of the flow around an elliptic stagnation point is always opposite to the rotation of the frame; this is generally called anticyclonic motion.[12,15]

C. Flow field for *N*=2

In configurations of two vortices on a disk, the vortex motion is always regular and integrable (i.e., nonchaotic).[6] Actually, in the frame rotating with vortex 1, vortex 2 describes regular trajectories following iso-lines of the Hamiltonian. For a derivation of this, the reader is referred to the Appendix . The period of the regular trajectory, which can be denoted by T_v, depends on the initial vortex positions and the vortex strengths.

The motion of passive tracers in configurations of two vortices on a disk is governed by the following stream function:

$$\Psi(r,\theta) = \sum_{j=1}^{2}\Gamma_j[\Psi_V(r,\theta,r_j,\theta_j) - \Psi_I(r,\theta,r_j,\theta_j)], \tag{15}$$

which depends on both the passive tracer position (r,θ) and the vortex positions (r_1,θ_1) and (r_2,θ_2). In the corotating frame the vortices have one degree of freedom less than in the fixed frame. Still, the remaining number of degrees of freedom is too large and the stream function is not integrable.[16] Thus, the advection of passive tracers in a two-vortex system on a disk is chaotic, except for a number of special cases.[6]

Besides chaotically moving passive tracers, some patches of regularly moving passive tracers can be found. These patches are called islands of regular motion, which can be either hyperbolic or elliptic. On the one hand, hyperbolic islands are situated around the point vortex centers. They persist even when the vortex motion itself is chaotic.[18] On the other hand, elliptic islands may arise in regions far away from vortex cores. Since these islands do not contain a singular vortex core, the relative velocity of passive tracers tends to zero in the center of the island; therefore, they are called elliptic islands.[7]

D. Equations of motion of heavy particles

The heavy particles in relevant applications (such as tiny iced droplets in gas-liquid separators) are small and approximately spherical. The mass loading is assumed to be suffi-

ciently small, so that particles do not influence the gas flow. Furthermore, effects of interparticle collisions are not taken into account. Hence, the approach presented here is based on a one-way coupling. The equation of motion for small spherical particles has been established by Maxey and Riley.[19] It comprises effects of a pressure gradient, an added mass term, the Stokes drag, the Basset history force, and buoyancy. In most practical applications with small, heavy particles, however, the Stokes drag and gravity are the dominant forces.[10,11] In order to isolate the phenomenon of heavy particles influenced by coherent vortices, gravity is also neglected, which is a reasonable approximation in view of several industrial applications. As a result, the equations of motion reduce to

$$\frac{d\boldsymbol{x}_p}{dt} = \boldsymbol{u}_p,$$

$$\frac{d\boldsymbol{u}_p}{dt} = \frac{1}{\mathrm{St}}(\boldsymbol{u}_g - \boldsymbol{u}_p), \tag{16}$$

where $\boldsymbol{x}_p$ and $\boldsymbol{u}_p$ are the position and the velocity of the particle, respectively, and $\boldsymbol{u}_g$ is the velocity of the gas. The parameter St is the Stokes number, which is the ratio between the particle relaxation time, τ_p, and the characteristic time scale of the flow, R^2/Γ_1,

$$\mathrm{St} = \frac{\tau_p \Gamma_1}{R^2}. \tag{17}$$

Particles with St=0 will react instantaneously to changes in the flow and will thus act as passive tracers, whereas particles with St$\rightarrow\infty$ will be insensitive to the flow field.

We rewrite the equations of motion in a rotating reference frame,

$$\frac{d\boldsymbol{\xi}_p}{dt} = \boldsymbol{v}_p, \tag{18}$$

$$\frac{d\boldsymbol{v}_p}{dt} = \frac{1}{\mathrm{St}}(\boldsymbol{v}_g - \boldsymbol{v}_p) - 2\boldsymbol{\Omega} \wedge \boldsymbol{v}_p + \Omega^2 \boldsymbol{\xi}_p - \dot{\boldsymbol{\Omega}} \wedge \boldsymbol{\xi}_p, \tag{19}$$

where $\boldsymbol{\xi}$ and $\boldsymbol{v}$ denote the position and the velocity in the rotating frame, respectively. The additional terms on the right-hand side, which all depend on the rotation rate Ω and its time derivative $\dot{\Omega}$, denote the Coriolis force, the centrifugal force, and an additional force due to the acceleration of the reference frame, respectively. The specific choice of Ω depends on the situation at hand.

We consider the trajectories of two nearby particles. The differences in position and velocity are denoted by $\delta\boldsymbol{\xi}_p$ and $\delta\boldsymbol{v}_p$, respectively. When the magnitude of the four-dimensional separation vector $\boldsymbol{R} \equiv [\delta\boldsymbol{\xi}_p, \delta\boldsymbol{v}_p]^T$ (Ref. 20) is very small, the separation between the two trajectories can be expressed in the following form:

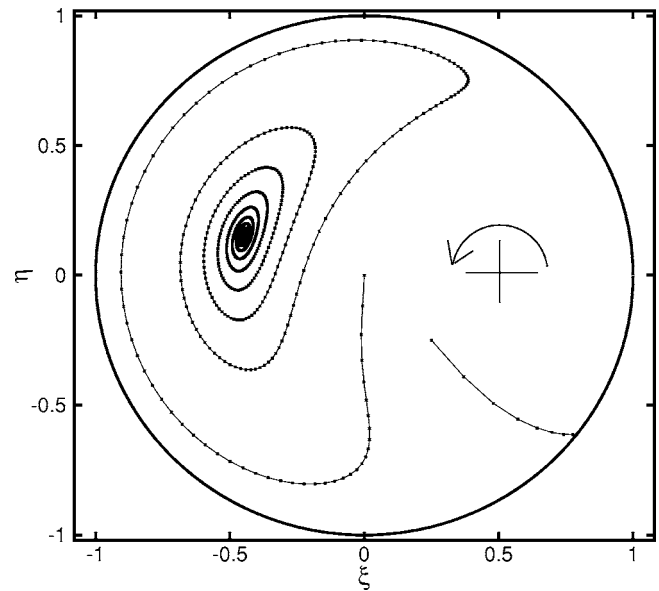$$\frac{d}{dt}\boldsymbol{R}(t) = \boldsymbol{M}\boldsymbol{R}(t), \tag{20}$$

with

FIG. 3. Trajectories of two slipping particles in a one-vortex system; $L^2=0.25$; St=0.5. The initial positions of the two particles are $(\xi,\eta)|_{t=0} = (0,0)$ and $(\xi,\eta)|_{t=0} = (0.25, -0.25)$.

$$\boldsymbol{M} = \begin{pmatrix} 0 & 0 & 1 & 0 \\ 0 & 0 & 0 & 1 \\ \dfrac{1}{\mathrm{St}}\dfrac{\partial v_g}{\partial \xi} + \Omega^2 & \dfrac{1}{\mathrm{St}}\dfrac{\partial v_g}{\partial \eta} + \dot{\Omega} & -\dfrac{1}{\mathrm{St}} & 2\Omega \\ \dfrac{1}{\mathrm{St}}\dfrac{\partial v_g}{\partial \xi} - \dot{\Omega} & \dfrac{1}{\mathrm{St}}\dfrac{\partial v_g}{\partial \eta} + \Omega^2 & -2\Omega & -\dfrac{1}{\mathrm{St}} \end{pmatrix}. \tag{21}$$

When all eigenvalues of the matrix $\boldsymbol{M}$ have a real part smaller than zero, we have $|\boldsymbol{R}(t)| \rightarrow 0$ for $t \rightarrow \infty$. This means that the two particles converge for sufficiently large times.

III. HEAVY PARTICLES IN BOUNDED ONE-VORTEX FLOW

In this section we consider the motion of heavy particles in a system with only one vortex. We conduct a numerical simulation where each particle is traced individually by using a fourth-order Runge-Kutta method. The equations of motion, Eq. (16), are solved for a series of decreasing values of the time step, where each next value is half of the previous value. When the differences between two subsequent solutions are below a certain preset level, the last obtained solution is considered sufficiently accurate. At the start of the simulation, the particles have the same velocity as the local gas flow. When a particle reaches the circular boundary, it is absorbed by the wall.

In Fig. 3, two different particle trajectories in the frame corotating with the vortex are plotted for $L^2=0.25$ (equiva-
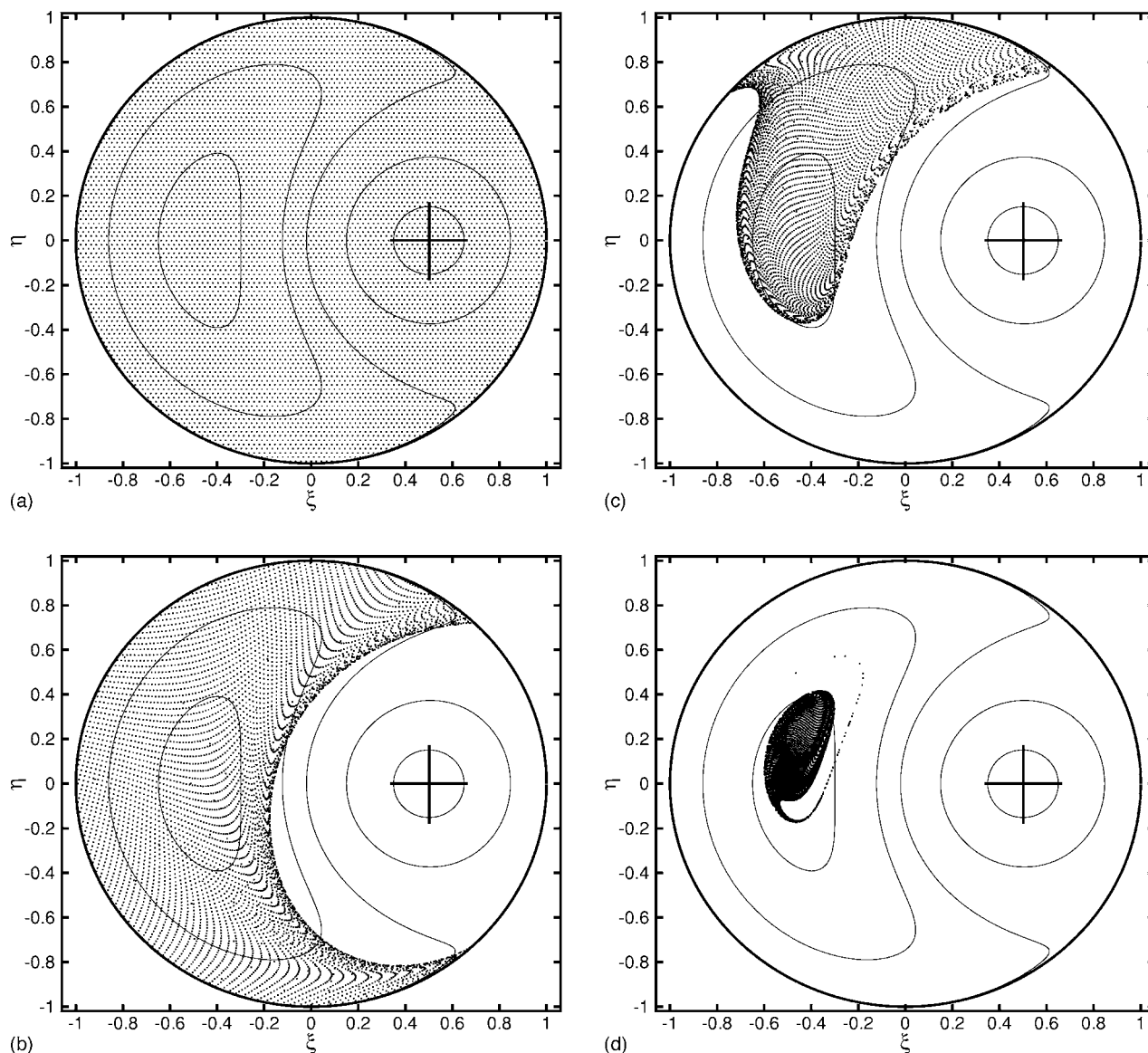
FIG. 4. Positions of heavy particles in one-vortex system; $L^2=0.25$, St=0.5: (a) $t=0$; (b) $t=5$; (c) $t=25$; (d) $t=100$. Streamlines of passive tracers are plotted in the background.

lent to $r_1=0.5$). Two regimes of particle motion can be distinguished in Fig. 3: either a particle is quickly expelled from the circular domain and is absorbed by the wall, or a particle is attracted to a point within the circular domain. Since we are observing the flow in a frame corotating with the vortex, the attraction point corresponds to a circular trajectory periodic with the vortex motion in a fixed frame.

In Fig. 4, the positions of a large number of particles are plotted for four instants in (dimensionless) time: $t=0$, $t=5$, $t=25$, and $t=100$. The 7495 particles, which all have the same Stokes number, St=0.5, are uniformly distributed at the start of the simulation ($t=0$). For large times, particles are trapped in a region around the attraction point.

The particle trapping efficiency P, defined as

$$P \equiv \frac{(\text{number of particles with } r<1 \text{ for } t \rightarrow \infty)}{(\text{total number of initially uniformly distributed particles})} \times 100 \%, \tag{22}$$

is plotted in Fig. 5, for three different configurations of bounded one-vortex flow: $L^2=0.09$, $L^2=0.25$, and $L^2=0.49$.

Figure 5 shows that the particle trapping phenomenon becomes more important for larger values of the angular mo-
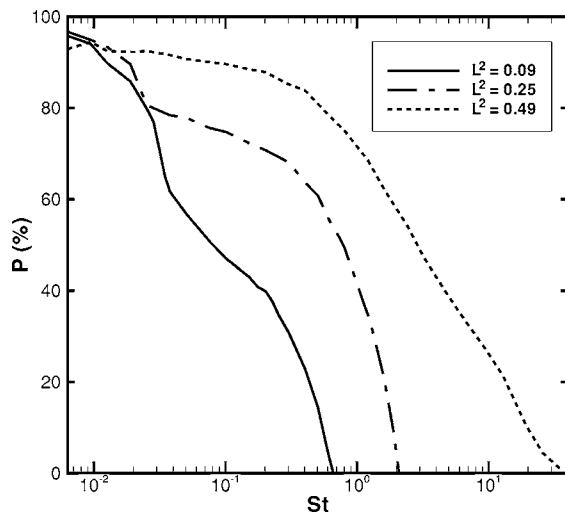
FIG. 5. Percentage of accumulated particles in a one-vortex system as a function of St, for three different one-vortex configurations: $L^2=0.09$, $L^2=0.25$, and $L^2=0.49$.

FIG. 6. Positions of trapped particles in a one-vortex system, obtained from numerical simulations; ■: St=0.1, ▲: St=0.3, ▼: St=0.6, ♦: St=0.9. The dashed line depicts the exact locations of fixed points.

mentum L^2 and for smaller values of the Stokes number. For sufficiently large values of the Stokes number $P=0$, i.e., accumulation is not present.

For particle accumulation to occur, two conditions must be met:

(i)   a fixed point must exist, and
(ii)   the fixed point must be stable.

In the remainder of this section, these two conditions are investigated.

A. Location of fixed points

Since the corotation is steady and equal to the angular velocity of vortex 1, i.e., $\Omega=\dot{\theta}_1$ and $\dot{\Omega}=0$, Eqs. (19) reduce to

$$\frac{d\boldsymbol{\xi}_p}{dt} = \boldsymbol{v}_p,$$

$$\frac{d\boldsymbol{v}_p}{dt} = \frac{1}{\text{St}}(\boldsymbol{v}_g - \boldsymbol{v}_p) - 2\dot{\theta}_1 \wedge \boldsymbol{v}_p + \dot{\theta}_1^2 \boldsymbol{\xi}_p. \tag{23}$$

The flow field $\boldsymbol{v}_g$ is time independent in this corotating frame. In a fixed point, say $\boldsymbol{\xi}^*$, we have $\boldsymbol{v}_p(\boldsymbol{\xi}^*)=0$, and the Stokes drag balances the centrifugal acceleration,

$$\boldsymbol{v}_g(\boldsymbol{\xi}^*) + \text{St}\ \dot{\theta}_1^2 \boldsymbol{\xi}^* = 0. \tag{24}$$

Writing $\xi^*=r^*\cos\phi^*$ and $\eta^*=r^*\sin\phi^*$, we have for the velocity components in ϕ and r directions, respectively,

$$u_\phi(r^*,\phi^*;r_1) = 0, \tag{25}$$

$$u_r(r^*,\phi^*;r_1) = -\text{St}\ \dot{\theta}_1^2 r^*. \tag{26}$$

For given r_1 and St, these two equations can be solved for r^* and ϕ^*. To facilitate the actual computation of (r^*,ϕ^*), it is convenient to solve Eq. (25) for $\cos\phi^*$,
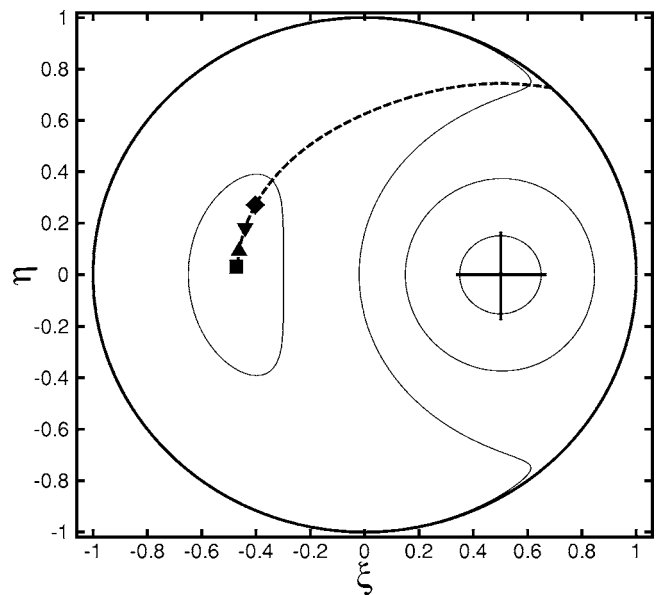
$$\cos\phi^* = \frac{-b \pm \sqrt{b^2-4ac}}{2a}, \tag{27}$$

where

$$a = -8\pi\dot{\theta}_1 r_1^2 r^{*3}, \tag{28}$$

$$b = 4\pi\dot{\theta}_1(r_1 r^{*4} + r_1^3 r^{*2} + r_1 r^{*2} + r_1^3 r^{*4}) + r_1^3 - r_1 + r_1^3 r^{*2} \\ - r_1 r^{*2}, \tag{29}$$

$$c = -2\pi\dot{\theta}_1(r^{*3} + r_1^2 r^* + r_1^2 r^{*4} + r_1^4 r^{*3}) + r^* - r_1^4 r^*. \tag{30}$$

The results are presented in Fig. 6 for $r_1=0.5$ and varying St, together with data obtained from numerical simulations for St=0.1, St=0.3, St=0.6, and St=0.9, showing excellent agreement.

For small Stokes numbers, the distance of the fixed point with respect to the stagnation point can be approximated in closed form. From Eq. (24), it follows that

$$\lim_{\text{St}\downarrow 0}|\boldsymbol{\xi}^* - \boldsymbol{\xi}_0| = 0, \tag{31}$$

where $\boldsymbol{\xi}_0$ is a stagnation point of the flow. This must be the elliptic stagnation point situated on the negative ξ axis (point E in Fig. 2), since the hyperbolic stagnation points (i.e., saddle points of the stream function) are essentially unstable, which is shown in the next section. The ξ component of Eq. (24) becomes

$$\left(\frac{\partial^2 \hat{\Psi}}{\partial \eta^2}\bigg|_{\xi_0}\right)(\eta^* - \eta_0) + \text{St}\ \dot{\theta}_1^2 \xi_0 + \mathcal{O}(\text{St}^2) = 0, \tag{32}$$
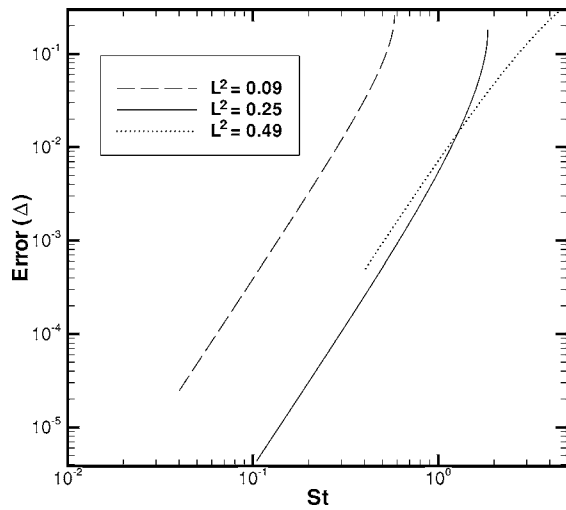
and it follows that

FIG. 7. Difference between the distance Δ obtained from the approximate equation Eq. (33), and the exact value, as a function of the Stokes number.
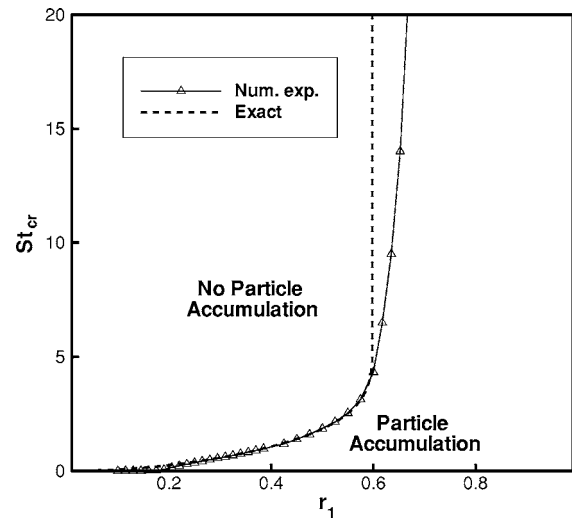

FIG. 8. Critical Stokes number as a function of the vortex position r_1 $(=\sqrt{L^2})$; the solid line with small triangles is the result of numerical experiments; the dashed line is determined from Eq. (38).

$$\Delta \equiv |\boldsymbol{\xi}^* - \boldsymbol{\xi}_0| = \text{St}\, \dot{\theta}_1^2 |\boldsymbol{\xi}_0| \left(\left. \frac{\partial^2 \hat{\Psi}}{\partial \eta^2} \right|_{\xi_0} \right)^{-1} + \mathcal{O}(\text{St}^2). \quad (33)$$

The physical reason for this is that larger particles (larger Stokes number) will slip more with respect to the carrier flow than smaller particles (smaller Stokes number). In order to balance the larger centrifugal force with the drag force, the fixed point needs to be situated further away from the elliptic point, where the carrier flow velocity is larger.

We have compared the values of Δ obtained from the approximation $\Delta \propto \text{St}$ [Eq. (33)] with the exact values based on solution of Eqs. (25) and (26). The deviation between the two solutions is plotted in Fig. 7 as a function of St for three different values of r_1. Indeed, for small Stokes numbers the error is relatively low in all three vortex configurations, so the approximation presented in (33) is accurate. Moreover, the error goes to zero as $\text{St} \downarrow 0$, confirming the consistency of the approximation.

B. Stability of fixed points

In this section the stability of the fixed point $\boldsymbol{\xi}^*$ is assessed by means of a linear stability analysis. When the particle is sufficiently close to the attraction point, the equation of motion can be approximated by

$$\frac{d}{dt} \boldsymbol{R}^*(t) = \boldsymbol{M}^* \boldsymbol{R}^*(t), \quad (34)$$

where $\boldsymbol{R}^*$ is a vector denoting the separation between the particle and the fixed point (in $\mathbb{R}^4$),

$$\boldsymbol{R}^* \equiv [\boldsymbol{\xi}_p - \boldsymbol{\xi}^*, \boldsymbol{v}_p]^T, \quad (35)$$

and $\boldsymbol{M}^*$ is the matrix $\boldsymbol{M}$ defined by Eq. (21), evaluated in $\boldsymbol{\xi}^*$. In the present case of one vortex, the matrix $\boldsymbol{M}^*$ is independent of time. When the real parts of all eigenvalues $\lambda_1, \ldots, \lambda_4$ of $\boldsymbol{M}^*$ are negative, then $|\boldsymbol{R}^*| \to 0$ for $t \to \infty$, and the fixed point $\boldsymbol{\xi}^*$ is an attraction point. Hence, we define a *stable fixed point* as a fixed point which satisfies

$$\max_k \text{Re}(\lambda_k) < 0. \quad (36)$$

The eigenvalues λ_k are the roots of the characteristic polynomial of $\boldsymbol{M}^*$,

$$\text{St}^2 \lambda^4 + 2\, \text{St}\, \lambda^3 + (2\, \text{St}^2\, \dot{\theta}_1^2 + 1)\lambda^2 + 2\, \text{St}\, \dot{\theta}_1^2 \lambda + \text{St}^2\, \dot{\theta}_1^4$$
$$+ \mathcal{H}^* = 0, \quad (37)$$

where $\mathcal{H}^*$ is the Hessian defined in Eq. (13), evaluated in the fixed point $\boldsymbol{\xi}^*$. The solutions are

$$\lambda_{1,2,3,4} = \frac{-1 \pm \sqrt{1 - 4 \dot{\theta}_1^2\, \text{St}^2 \pm 4i\, \text{St}\sqrt{\mathcal{H}^*}}}{2\, \text{St}}. \quad (38)$$

We start to analyze the eigenvalues in the limit of $\text{St} \downarrow 0$, and expand Eq. (38),

$$\lambda_{1,2,3,4} = \frac{-1 \pm 1}{2\, \text{St}} + \text{St}(\mathcal{H}^* - \dot{\theta}_1^2) \pm i\sqrt{\mathcal{H}^*} + \mathcal{O}(\text{St}^2). \quad (39)$$

In the previous section we found that $|\boldsymbol{\xi}^* - \boldsymbol{\xi}_0| = \mathcal{O}(\text{St})$; hence, $\mathcal{H}^* = \mathcal{H}_0 + \mathcal{O}(\text{St})$, and

$$\lambda_{1,2,3,4} = \frac{-1 \pm 1}{2\, \text{St}} + \text{St}(\mathcal{H}_0 - \dot{\theta}_1^2) \pm i\sqrt{\mathcal{H}_0} + i\mathcal{O}(\text{St})$$
$$+ \mathcal{O}(\text{St}^2). \quad (40)$$

We assume that the fixed point at hand belongs to a curve of stable fixed points $\boldsymbol{\xi}^*(\text{St}; r_1)$ with $\boldsymbol{\xi}^*(0; r_1) = \boldsymbol{\xi}_0(r_1)$, i.e., when $\text{St} \downarrow 0$ the fixed point tends to a stagnation point. If $\mathcal{H}_0 < 0$ then $i\sqrt{\mathcal{H}_0} \in \mathbb{R}$ and the fixed point cannot be stable for $\text{St} \downarrow 0$. Therefore, we require $\mathcal{H}_0 > 0$ as a necessary condition, i.e., the stagnation point must be elliptic. Furthermore, from Eq.

(14) we observe that $(\mathcal{H}^* - \dot{\theta}_1^2) < 0$, and therefore the condition $\mathcal{H}_0 > 0$ is also sufficient for the fixed point to be stable. It is noted that the real parts of the eigenvalues, if all negative, describe the rate at which a particle moves towards the fixed point, which is apparently linear in the Stokes number. Therefore, the particle trapping time is inversely proportional to the Stokes number.

We continue by analyzing the eigenvalues for arbitrary values of the Stokes number. Upon definition of the following two variables:

$$A \equiv 1 - 4\dot{\theta}_1^2 \, \mathrm{St}^2, \quad B \equiv 4 \, \mathrm{St}\sqrt{|\mathcal{H}^*|}, \tag{41}$$

we observe that

$$\max_k \mathrm{Re}(\lambda_k) = \begin{cases} \dfrac{-1 + \sqrt{\dfrac{1}{2}A + \dfrac{1}{2}\sqrt{A^2 + B^2}}}{2\,\mathrm{St}}, & \mathcal{H}^* > 0, \\[20pt] -\dfrac{1}{2\,\mathrm{St}}, & \mathcal{H}^* < 0 \quad A + B < 0, \\[14pt] \dfrac{-1 + \sqrt{A + B}}{2\,\mathrm{St}}, & \mathcal{H}^* < 0 \quad A + B > 0. \end{cases} \tag{42}$$

From these observations we derive the following sufficient stability conditions:

$$\mathcal{H}^* < 0 \text{ and } A + B < 1 \Rightarrow \max_k \mathrm{Re}(\lambda_k) < 0, \tag{43}$$

$$\mathcal{H}^* > 0 \text{ and } A + \sqrt{A^2 + B^2} < 2 \Rightarrow \max_k \mathrm{Re}(\lambda_k) < 0. \tag{44}$$

Finally, we determine $\mathrm{St}_{cr}(r_1)$, the maximum value of St for which a stable fixed point can be found. For given r_1 we identify the set $\mu(r_1)$ of points (r_1, r^*), where $\max_k \mathrm{Re}[\lambda_k(r_1, r^*)] < 0$, i.e., where fixed points are stable. Then, we determine the maximum value of the Stokes number over the set $\mu(r_1)$; this is $\mathrm{St}_{cr}(r_1)$. We note that for each (r_1, r^*) one finds two values for $\cos \phi^*$ by Eq. (27). Whenever both values lead to stable fixed points, we take into account the value that results in the largest value of St. The critical Stokes number can also be determined numerically by repeating the simulation of particles for a wide range of Stokes numbers at a given r_1: the smallest value of the Stokes number for which no accumulation takes place is $\mathrm{St}_{cr}(r_1)$.

The numerically obtained data set for St_{cr} is compared to the exact formulation in Fig. 8. From $r_1 > 0.6$, the critical Stokes number becomes infinite according to the exact formulation. In the numerical simulations, however, the critical Stokes number remains finite, although it increases very quickly as $r_1 > 0.6$. The reason for the deviation of the numerical results is that, for a finite number of particles in phase space (position *and* velocity), there may be no particles close enough to the attraction point. Still, it is clear from the exact curve for St_{cr} that small, heavy particles may always accumulate inside the circular domain, and that this phenomenon becomes more important as r_1 increases.

The stability criterion derived in Eq. (38) is evidently not restricted to the flow induced by a point vortex in a circular

domain. It can be applied to any incompressible flow, as long as it is steady in some steadily rotating reference frame. Examples of this comprise the motion of vortices on a regular polygon on an infinite plane or on a disk (whose origin coincides with the barycenter) or an approximation of the flow field on a Keplerian disk as given by Chavanis.[14] Chavanis prescribes an anticyclonic vortex region *a priori*; in our case, the elliptic island is formed naturally just by the presence of a vortex inside a circular boundary.

IV. HEAVY PARTICLES IN BOUNDED TWO-VORTEX FLOW

We consider the motion of heavy particles in a flow generated by two equal point vortices in a circular domain. In order to visualize the results for heavy particles, four vortex configurations are investigated in particular. The first configuration, with $L^2 = 0.18$, is the same as was treated by Boffetta *et al.*;[6] the vortex positions are initially:

$$(r_1, \theta_1) = \left(\frac{\sqrt{2}}{10}, 0\right), \quad \text{on } t = 0,$$

$$(r_2, \theta_2) = \left(\frac{2}{5}, \pi\right), \quad \text{on } t = 0.$$

The case with $L^2 = 0.37$ corresponds to the following initial vortex positions:

$$(r_1, \theta_1) = \left(\frac{1}{10}, 0\right), \quad \text{on } t = 0,$$

$$(r_2, \theta_2) = \left(\frac{6}{10}, 0\right), \quad \text{on } t = 0.$$

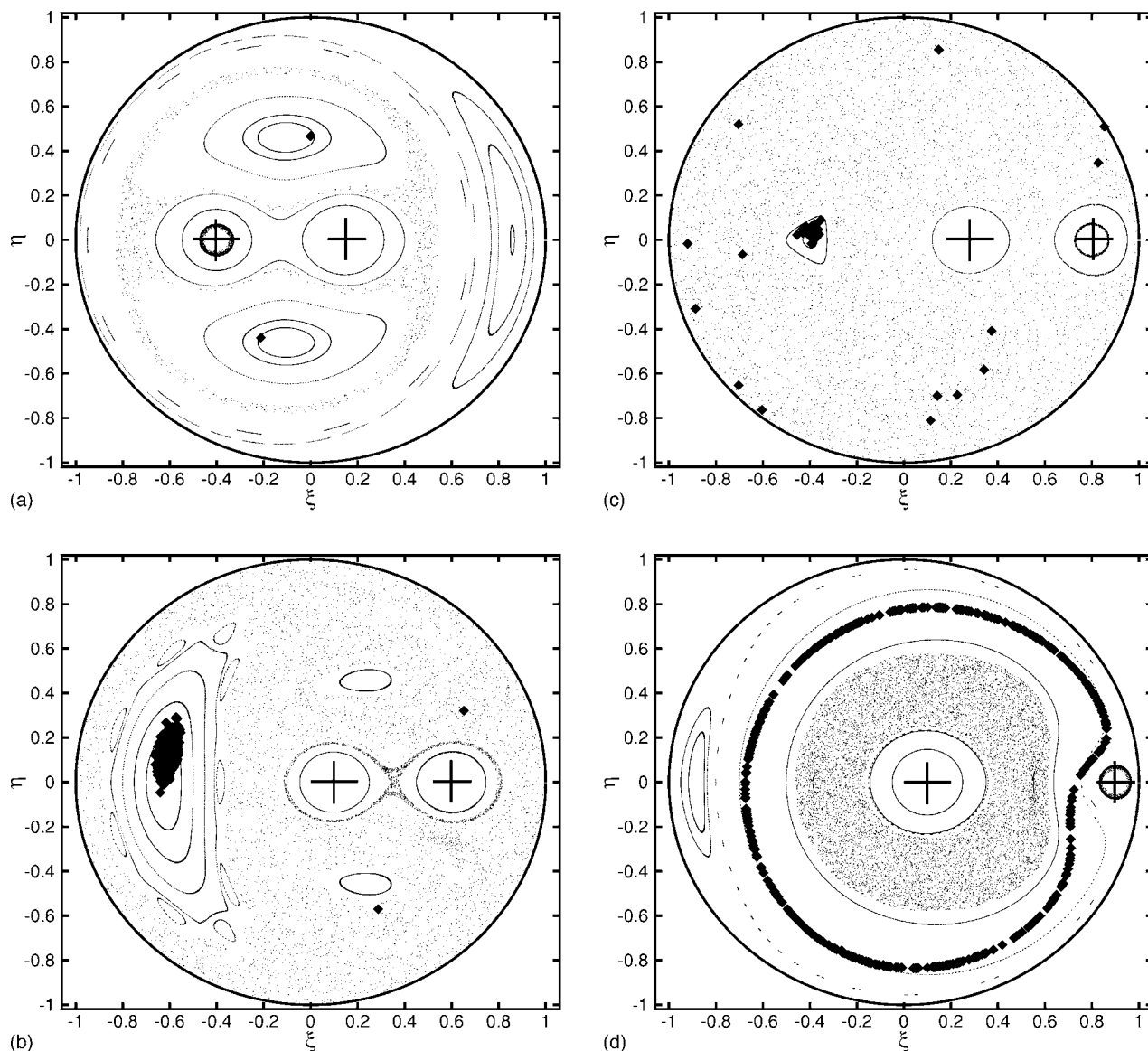In the configuration with $L^2 = 0.72$, the initial vortex positions are chosen to be

FIG. 9. Positions of heavy particles (diamonds) in two-vortex system after time $t=nT_v \simeq 100$, $n \in \mathbb{N}$; St=0.1: (a) $L^2=0.18$; (b) $L^2=0.37$; (c) $L^2=0.72$; (d) $L^2=0.82$. For comparison, Poincaré sections of $\mathcal{O}(10)$ different passive tracers (small dots) are plotted, too.

$$(r_1, \theta_1) = \left(\frac{\sqrt{2}}{5}, 0 \right), \quad \text{on } t=0$$

$$(r_2, \theta_2) = \left(\frac{4}{5}, 0 \right), \quad \text{on } t=0.$$

Finally, a configuration is treated with $L^2=0.82$, where the initial vortex positions are

$$(r_1, \theta_1) = \left(\frac{1}{10}, 0 \right), \quad \text{on } t=0$$

$$(r_2, \theta_2) = \left(\frac{9}{10}, 0 \right), \quad \text{on } t=0.$$

First, we consider the motion of passive tracers in the four configurations. Poincaré sections of passive tracer positions with interval T_v are plotted in Fig. 9; passive tracers are represented by small dots. The passive tracers can be classi-

fied into three groups: hyperbolic islands, elliptic islands, and chaotic regions. In all configurations two hyperbolic islands can be recognized on the ξ axis, around the point vortex centers; the chaotic regions can be recognized from the random distribution of passive tracers. In addition, some elliptic islands occur. In Fig. 9(a), the two most important elliptic islands are situated around $(\xi, \eta) \simeq (-0.1, \pm 0.5)$. Three elliptic islands can be identified in Fig. 9(b), on $(\xi, \eta) \simeq (0.1, \pm 0.5)$ and on $(\xi, \eta) \simeq (-0.6, 0.0)$. In Fig. 9(c), only one elliptic island is visible, on $(\xi, \eta) \simeq (-0.4, 0)$. Finally, in Fig. 9(d), an almost circular anticyclonic region of regular motion is found between the two vortices. There is, however, no point in this region where the relative velocity of passive tracers goes to zero.

In Fig. 9, the positions of heavy particles are presented too. The initially uniformly distributed particles, with St $=0.1$, are plotted after $t=nT_v \simeq 100$, $n \in \mathbb{N}$. Thus, the heavy particles are plotted on the moment that the two vortices
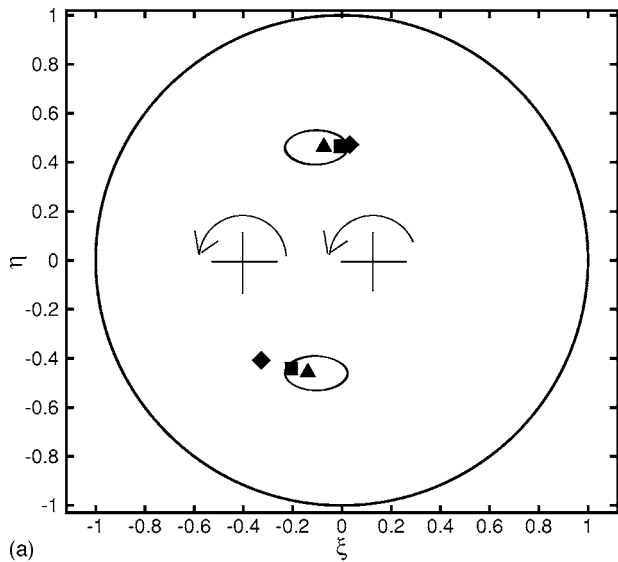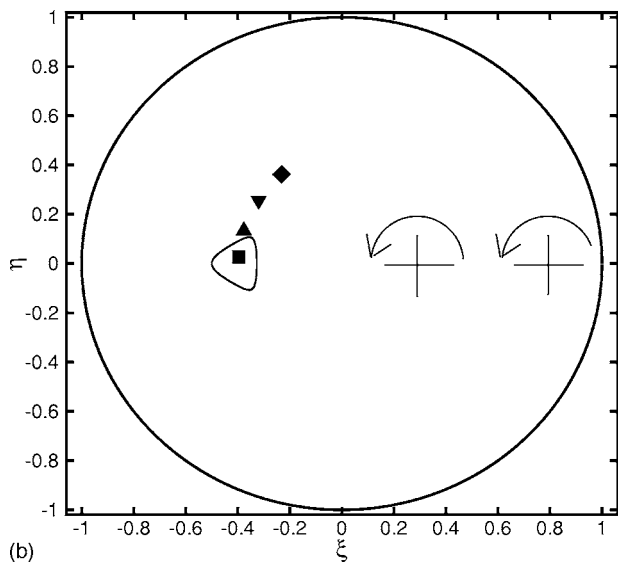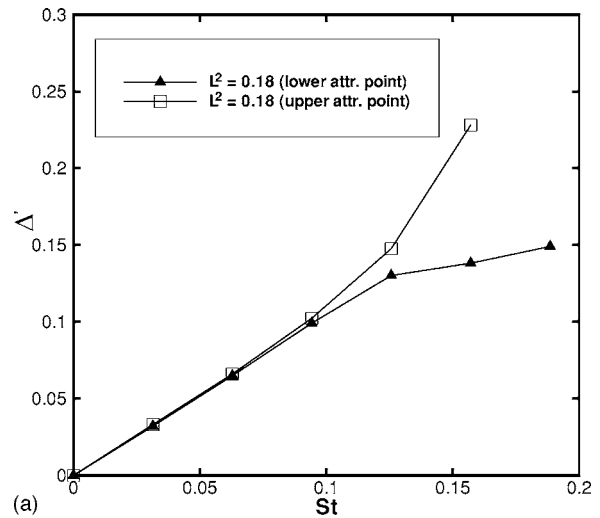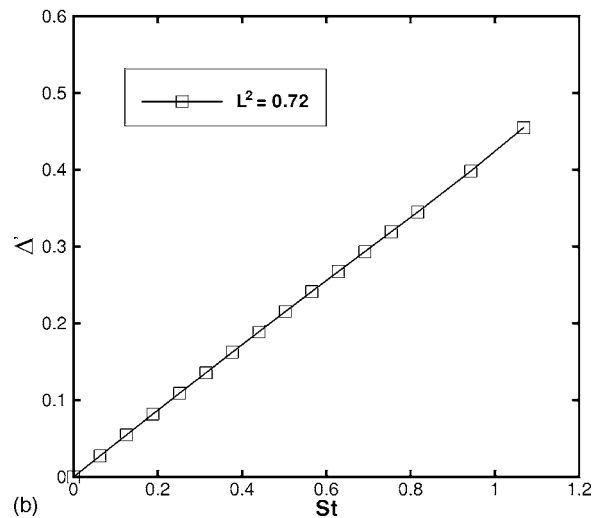
FIG. 10. Poincaré sections with period T_v of particles trapped in the moving attraction points: (a) $L^2=0.18$; ▲: St=0.03, ■: St=0.09, ◆: St=0.15; (b) $L^2=0.72$; ■: St=0.1, ▲: St=0.3, ▼: St=0.6, ◆: St=0.9.

FIG. 11. Distance between a trapped particle and the center of the elliptic island Δ' as a function of the Stokes number, on the moment that the two vortices have zero relative angle: (a) $L^2=0.18$; (b) $L^2=0.72$.

have zero relative angle, i.e., the vortices have the same relative positions as on $t=0$. In the configuration with $L^2=0.18$, a large number of particles have accumulated in two single points near the elliptic islands; all other particles have been expelled from the domain. The case of $L^2=0.37$ is similar, since many particles have either accumulated close to the small elliptic islands or in the big elliptic island in the left half-plane. In the case $L^2=0.72$, some particles are trapped close to the elliptic island in the left half-plane; a few others are still in the chaotic sea. In longer simulations it is observed that the dispersed particles eventually reach the wall, whereas the trapped particles accumulate in the elliptic island. The trapped particles in all these examples are attracted towards a regular trajectory which is in phase with the vortex motion. In the two-vortex system, the attraction point is not a fixed point like in the one-vortex system; it is better to speak of a moving attraction point instead.

In the case of $L^2=0.82$, no elliptic island exists to which

the heavy particles can be attracted. The anticyclonic region of regular passive tracer motion, however, does attract particles that are expelled from the regions around the vortices; as $t \to \infty$ heavy particles can be found on a closed line [see Fig. 9(d)].

A. Location of moving attraction point

For the particle accumulation to occur in the two-vortex system, a force-balanced periodically moving attraction point has to exist with respect to the vortex motion. First, this requires the existence of a regular motion of the heavy particles with respect to the vortices. This regular motion is not straightforward to find because of the unsteadiness of the flow field. Still, it is known that in the limit of St↓0, the motion of heavy particles corresponds to the motion of passive tracers. So, the moving attraction point of heavy particles should go to a point of regular motion of passive tracers as their Stokes number vanishes. Hence, just like the case of one vortex, the particle accumulation takes place around the centers of elliptic islands.
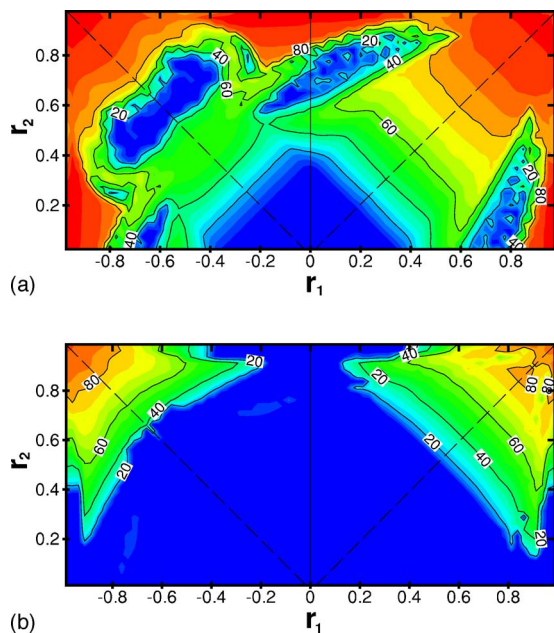
FIG. 12. Percentage P of accumulated heavy particles as a function of the two-vortex configuration (r_1, r_2); (a) St=0.1; (b) St=1.

The shape of the elliptic islands is in phase with the vortex motion. The same holds for the trajectory of trapped heavy particles. Therefore, both a trapped particle and the center of the elliptic island are on the same position after every vortex period. Poincaré sections with time T_v can then visualize the influence of the Stokes number on the position of the moving attraction point. The results are presented in Fig. 10, for the cases of $L^2 = 0.18$ and $L^2 = 0.72$. In both cases, the center of the elliptic island is plotted too. Clearly, the location of the moving attraction point is increasingly far away from the center of the elliptic island for higher Stokes numbers.

Some particles with higher Stokes numbers even have a fixed point in a region outside of the elliptic islands, as can be observed for three particles in Fig. 10(b). This means that these heavy particles describe a regular motion, in period with the vortex motion, although they are surrounded by cha-

otically moving passive tracers. This seems rather contradictory but this phenomenon can be explained from the dissipative nature of the governing equations of motion [Eq. (16)]: whereas passive tracer motion is governed by a Hamiltonian that conserves the phase-space volume, the phase-space volume of heavy particles goes to zero for $t \to \infty$.[21]

In Fig. 11, the distance Δ' is shown as a function of the Stokes number. Here, Δ' is defined as

$$\Delta' \equiv [|\boldsymbol{\xi}_p^*(t) - \boldsymbol{\xi}_0(t)|]_{t=nT_v}, \quad n \in \mathbb{N}, \tag{45}$$

which is the distance between the moving attraction point and the center of the elliptic island, on the moment that the two vortices have zero relative angle. The distance Δ' grows approximately linearly in the Stokes number, as long as the Stokes number is small enough. These results are very similar to the results of the one-vortex case.

B. Stability of moving attraction point

The stability of the moving attraction point can be investigated by using the separation vector from Eq. (20), where the time-dependent matrix $\boldsymbol{M}$ is given by Eq. (21) and evaluated at the moving attraction point. In Fig. 11 we found that $\Delta' \propto$ St, indicating that the moving attraction point is located close to the center of an elliptic island for small values of the Stokes number. Therefore, it is convenient to take the reference frame corotating with the center of the elliptic island, whose angular velocity is denoted by Ω_0 and its angular acceleration by $\dot{\Omega}_0$. The eigenvalues of $\boldsymbol{M}$ then follow from the (time-dependent) characteristic polynomial,

$$\text{St}^2 \lambda^4 + 2 \text{ St} \lambda^3 + (2 \text{ St}^2 \Omega_0^2 + 1)\lambda^2 + (2 \text{ St} \Omega_0^2$$
$$+ 4 \text{ St}^2 \Omega_0 \dot{\Omega}_0)\lambda + \text{ St}^2 \Omega_0^4 + \text{St}^2 \dot{\Omega}_0^2 + \mathcal{H}^* = 0. \tag{46}$$

In the limit of small relative acceleration compared to the inverse of the Stokes number, i.e.,

$$\left| \frac{\dot{\Omega}_0}{\Omega_0} \right| \ll \frac{1}{\text{St}}, \quad \forall\, t, \tag{47}$$

the eigenvalues become

$$\lambda_{1,2,3,4} \approx \frac{-1 \pm \sqrt{1 - 4\Omega_0^2 \text{St}^2 \pm 4\, \text{St}\sqrt{-\mathcal{H}^*(t) - 2\, \text{St}\, \Omega_0 \dot{\Omega}_0 - \text{St}^2\, \dot{\Omega}_0^2}}}{2\, \text{St}}. \tag{48}$$

In the two-vortex case, the Hessian $\mathcal{H}^*$ is strictly positive in the elliptic island for all time. Linearizing with respect to St, and making use of Eq. (47) then gives

$$\lambda_{1,2,3,4} \approx \frac{-1 \pm 1}{2\, \text{St}} + \text{St}(\mathcal{H}^* - \Omega_0^2) \pm i\sqrt{\mathcal{H}^*} + \mathcal{O}(\text{St}^2). \tag{49}$$

In Fig. 11 it was shown that approximately $\mathcal{H}^* = \mathcal{H}_0 + \mathcal{O}(\text{St})$, such that

$$\lambda_{1,2,3,4} \approx \frac{-1 \pm 1}{2\, \text{St}} + \text{St}(\mathcal{H}_0 - \Omega_0^2) \pm i\sqrt{\mathcal{H}_0} + i\mathcal{O}(\text{St})$$
$$+ \mathcal{O}(\text{St}^2). \tag{50}$$

A completely similar reasoning as is conducted in Sec. III, based on the observation that $(\mathcal{H}^* - \Omega_0^2) < 0$, leads to the conclusion that the condition $\mathcal{H}_0 > 0$ is both necessary and suf-
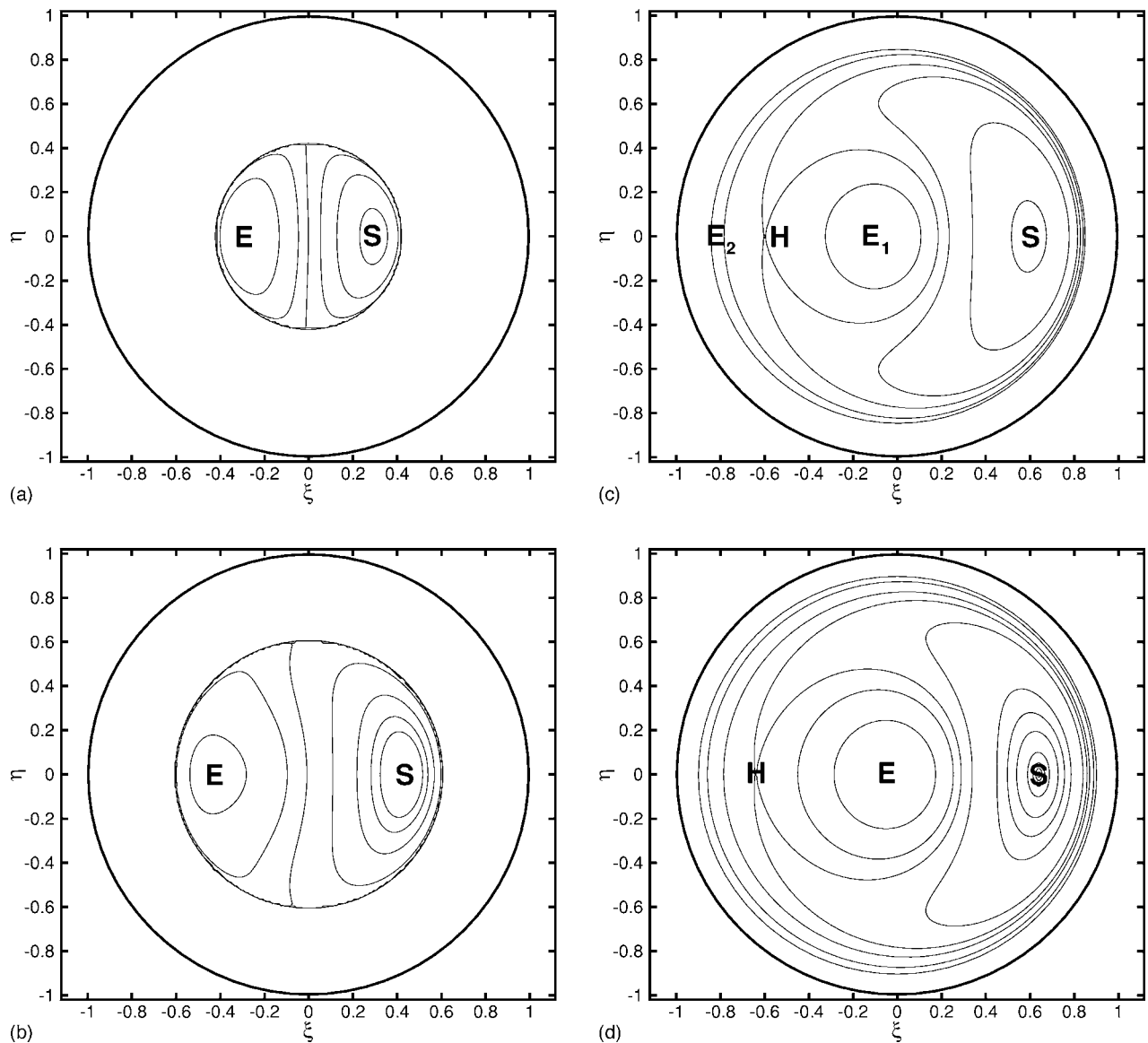
FIG. 13. Contour lines of Hamiltonian [Eq. (A4)] describing the motion of vortex 2 in the frame rotating with vortex 1. Both vortices have the same strength. E denotes a stable (elliptic) equilibrium configuration of the vortices, H is an unstable (hyperbolic) equilibrium configuration, and S is the singular configuration of two coinciding vortices: (a) $L^2=0.18$; (b) $L^2=0.37$; (c) $L^2=0.72$; (d) $L^2=0.82$.

ficient for the fixed point to be stable for small Stokes numbers. It is noted that the real parts of the eigenvalues are approximately linear in the Stokes number, so that the particle trapping time is inversely proportional to the Stokes number, just like in the one-vortex case.

The basin of attraction consists predominantly of heavy particles which are released in the regular elliptic islands. Also, from other regions of the flow, a large quantity of particles may eventually be forced towards the moving attraction point.

In order to quantify the particle accumulation, numerical simulations were done for a large variety of two-vortex configurations. For a range of 40×80 initial vortex positions (r_1, r_2), the positions of heavy particles are calculated after $t=500$, for two different Stokes numbers: St=0.1 and St=1. After such a long time, generally only the accumulated particles are present in the domain, whereas all other particles

have reached the wall. On the basis of these simulations, the parameter P, defined in Eq. (22), can be determined; the results are presented in Fig. 12 as a function of the vortex configuration r_1 and r_2. Since r_1 and r_2 may be interchanged without any consequence for the flow, the figures are symmetric around the lines $r_2=\pm r_1$, which are drawn for convenience.

Generally, the accumulation of heavy particles is enhanced with higher angular momentum and lower Stokes numbers. The low percentage of particle accumulation in the left half-plane of Fig. 12(a) [especially around $(r_1, r_2)=(-0.7, 0.4)$, or $(r_1, r_2)=(-0.4, 0.7)$] can be explained by the fact that the motion of passive tracers is highly chaotic; no elliptic islands exist in these configurations. This supports the hypothesis that heavy particle accumulation in bounded two-vortex flows takes place in elliptic islands of regular passive tracer motion.

V. CONCLUSIONS

In this paper, the motion of heavy particles in a bounded point vortex flow is investigated both theoretically and numerically. The numerical simulations are based on a one-way coupling. In order to isolate the effect of inertia, only the Stokes drag is taken into account in the equations of motion.

The results reveal that heavy particles may accumulate in regions where the centrifugal and the drag forces acting on the particles balance each other, thus causing an equilibrium trajectory. Two cases have been studied: the situation with one vortex on a disk and the situation with two vortices on a disk. These configurations correspond to a flow induced by one or two slender vortex filaments in a pipe.

A linear stability analysis in the one-vortex case shows that particles are always attracted to a fixed point in an anticyclonic region, as long as the Stokes number is below a critical value. This critical Stokes number depends on the particular flow properties; in general, it is higher as the angular momentum of the vortex increases. The fixed point is situated further away from the center of the anticyclonic region as the Stokes number increases. The rate at which a particle approaches towards an attraction point is approximately linear in the Stokes number.

In a bounded two-vortex flow, where the vortices display a regular periodic motion, the results are similar: heavy particles with small but nonzero Stokes number accumulate on a moving attraction point within the circular domain. The moving attraction point is situated near the center of an elliptic island, i.e., a region of regular anticyclonic motion of passive tracers. The distance between the attraction orbit and the center of the elliptic island increases for larger Stokes numbers. Again, the rate at which a particle approaches the moving attraction point is approximately proportional to the Stokes number.

The results from this paper may be useful in several applications where a three-dimensional swirl flow can be approximated by a two-dimensional rotating flow, e.g., in industrial gas-liquid separators containing helical vortex filaments. The results from the present research give a global idea of the motion of heavy particles in such systems.

APPENDIX: VORTEX MOTION IN CASE *N*=2

The Hamiltonian formulation [Eq. (5)] in the case of two vortices is

$$H = \Gamma_1\Gamma_2\left[\Psi_V(r_1,\theta_1,r_2,\theta_2) - \Psi_I(r_1,\theta_1,r_2,\theta_2) + \frac{1}{4\pi}\ln r_2^2\right]$$
$$+ \frac{1}{4\pi}\sum_{i=1}^{2}\Gamma_i^2\ln[1-r_i^2]. \tag{A1}$$

Using the conservation of angular momentum, this four-degree-of-freedom Hamiltonian can be reduced to a system of two degrees of freedom. For this purpose, r_1 is written in terms of r_2 using the invariant L^2,

$$r_1 = \sqrt{\frac{L^2 - \Gamma_2 r_2^2}{\Gamma_1}}, \quad \frac{dr_1}{dr_2} = -\frac{\Gamma_2 r_2}{\Gamma_1 r_1}. \tag{A2}$$

Then, the Hamiltonian, Eq. (A1), can be written as follows:[6]

$$H(r_1,\theta_1,r_2,\theta_2) = \hat{H}(r_2,\phi_2), \tag{A3}$$

with

$$\hat{H}(r_2,\phi_2) = \frac{1}{4\pi}\Gamma_1^2\ln\left[1 - \frac{L^2}{\Gamma_1} + \frac{\Gamma_2 r_2^2}{\Gamma_1}\right] + \frac{1}{4\pi}\Gamma_2^2\ln[1-r_2^2]$$
$$- \frac{1}{4\pi}\Gamma_1\Gamma_2\ln[\Gamma_1\Gamma_2 r_2^2 + \Gamma_2(L^2 - \Gamma_2 r_2^2)$$
$$- 2\sqrt{\Gamma_1\Gamma_2^2 r_2^2(L^2 - \Gamma_2 r_2^2)}\cos\phi_2]$$
$$+ \frac{1}{4\pi}\Gamma_1\Gamma_2\ln[\Gamma_1\Gamma_2 + \Gamma_2 r_2^2(L^2 - \Gamma_2 r_2^2)$$
$$- 2\sqrt{\Gamma_1\Gamma_2^2 r_2^2(L^2 - \Gamma_2 r_2^2)}\cos\phi_2]. \tag{A4}$$

The time development of r_2 and ϕ_2 can be obtained from the canonical equations,

$$\Gamma_2\dot{r}_2 = \frac{1}{r_2}\frac{\partial\hat{H}}{\partial\phi_2}, \quad \Gamma_2 r_2\dot{\phi}_2 = -\frac{\partial\hat{H}}{\partial r_2}. \tag{A5}$$

The radial position of the first vortex, r_1, then follows directly from Eq. (A2).

The contour lines of the Hamiltonian [Eq. (A4)] in the case of two equally strong vortices are plotted in Fig. 13 for $L^2=0.18$, $L^2=0.37$, $L^2=0.72$, and $L^2=0.82$. In all figures, the contour lines correspond to trajectories of the second vortex in the frame rotating with the first vortex, which is placed on the positive ξ axis ($\phi_1 \equiv 0$). More details on these figures can be found in Boffetta *et al.*[6]

[1] A. K. Gupta, D. G. Lilley, and N. Syred, *Swirl Flows* (Abacus Press, London, 1984).
[2] R. Hagmeijer, R. H. A. IJzermans, and F. Put, "Solution of the general dynamic equation along approximate fluid trajectories generated by the method of moments," Phys. Fluids **17**, 056101 (2005).
[3] J. C. Hardin, "The velocity field induced by a helical vortex filament," Phys. Fluids **25**, 1949 (1982).
[4] S. V. Alekseenko, P. A. Kuibin, V. L. Okulov, and S. I. Shtork, "Helical vortices in swirl flow," J. Fluid Mech. **382**, 195 (1999).
[5] H. Lamb, *Hydrodynamics* (Cambridge University Press, Cambridge, 1932).
[6] G. Boffetta, A. Celani, and P. Franzese, "Trapping of passive tracers in a point vortex system," J. Phys. A **29**, 3749 (1996).
[7] L. Kuznetsov and G. M. Zaslavsky, "Regular and chaotic advection in the flow field of a three-vortex system," Phys. Rev. E **58**, 7330 (1998).
[8] O. A. Druzhinin, "Dynamics of concentration and vorticity modification in a cellular flow laden with solid heavy particles," Phys. Fluids **7**, 2132 (1995).
[9] M. R. Maxey, "On the advection of spherical and non-spherical particles in a non-uniform flow," Proc. R. Soc. London, Ser. A **333**, 289 (1990).
[10] B. Marcu, E. Meiburg, and P. K. Newton, "Dynamics of heavy particles in a Burgers vortex," Phys. Fluids **7**, 400 (1995).
[11] A. M. Gañán-Calvo and J. C. Lasheras, "The dynamics and mixing of small spherical particles in a plane, free shear layer," Phys. Fluids A **3**, 1207 (1991).
[12] A. Bracco, P. H. Chavanis, A. Provenzale, and E. A. Spiegel, "Particle aggregation in a turbulent Keplerian flow," Phys. Fluids **11**, 2280 (1999).

[13] P. Barge and J. Sommeria, "Did planet formation begin inside persistent gaseous vortices?" Astron. Astrophys. **295**, L1 (1995).

[14] P. H. Chavanis, "Trapping of dust by coherent vortices in the solar nebula," Astron. Astrophys. **356**, 1089 (2000).

[15] A. Provenzale, "Transport by coherent barotropic vortices," Annu. Rev. Fluid Mech. **31**, 55 (1999).

[16] P. K. Newton, *The N-vortex Problem—Analytical Techniques* (Springer-Verlag, Berlin, 2001).

[17] H. Aref and M. Brons, "On stagnation points and streamline topology in vortex flows," J. Fluid Mech. **370**, 1 (1998).

[18] A. Babiano, G. Boffetta, A. Provenzale, and A. Vulpiani, "Chaotic advection in point vortex models and two-dimensional turbulence," Phys. Fluids **6**, 2465 (1994).

[19] M. R. Maxey and J. J. Riley, "Equation of motion for a small rigid sphere in a nonuniform flow," Phys. Fluids **26**, 883 (1983).

[20] J. Bec, "Fractal clustering of inertial particles in random flows," Phys. Fluids **15**, L81 (2003).

[21] J. M. Ottino, *The Kinematics of Mixing: Stretching, Chaos and Transport* (Cambridge University Press, Cambridge, 1989).